Full Paper

Propellants, Explosives, Pyrotechnics

DOI: 10.1002/prep.201500267

Confocal Scanning Laser Microscopic Study of the RDX Defect Structure in Deformed Polymer-Bonded Explosives

Antoine E. D. M. van der Heijden*[a, b] and Richard H. B. Bouma[a]

Abstract: The influence of an explosion-driven deformation on the defect structure in RDX crystals embedded in a polymer-bonded explosive was investigated by means of confocal scanning laser microscopy. The images were compared to the defect structure in the as-received RDX grades, embedded in an epoxy resin. In this way it is possible to qualitatively analyze the changes in defect structure of the RDX crystals that were induced by the explosion-driven deformation. For the first time, these data therefore provide experimental confirmation of how shock waves mechanically interact with energetic crystals – a topic that, up to now, was only explored by means of simulations.

Keywords: Confocal scanning laser microscopy · RDX defect structure · Non-shock deformation · Polymer-bonded explosive

1 Introduction

In most applications of munitions only a minor mechanical deformation is imposed during launch without any negative effect on functioning of the munition item. However, in some applications the mechanical deformation is severe and there is a risk of premature functioning initiated by the mechanically induced deformation. For these situations, a better understanding of the non-shock initiation phenomena is the key to prevent accidents and premature functioning.

The mechanical response of explosives at conditions close to or beyond a mechanically induced initiation threshold can be studied by various experimental techniques, e.g. the Susan impact and friability test, spigot intrusion [1], the Steven impact test [2], and the set-back generator [3]. Bouma and van der Heijden [4] studied the mechanical deformation of a polymer-bonded explosive (PBX) and its sensitivity to ignition, applying two different methods to subject the PBX samples to a mechanical deformation, namely in a ballistic impact chamber (BIC) and an explosion-driven deformation test. In that study, an explosive composition, based on AFX-757, has been systematically varied by using Class 1 RDX from three different sources and with known differences in crystal quality. The three RDX grades had been selected out of a total of seven RDX grades that were used in the Reduced Sensitivity RDX Round Robin program [5]. A selection of these RDX grades has been subject of further characterization studies. Van der Heijden et al. [6] examined the fractured surfaces of cleaved RDX crystals from three RDX grades by means of scanning electron microscopy, identifying the presence of small voids and inclusions.

In another study impact tests have been performed with all seven RDX grades, showing that it is possible to distinguish shock-insensitive from shock-sensitive RDX crystals by the shape of the pressure curve that is measured in the BIC set-up [7]. Confocal scanning laser microscopy (CSLM) has been applied to the selected three RDX grades [8], and previously also to HMX [9]. CSLM is an essential, non-invasive tool for many biomedical imaging applications [10]. However, an increased interest in the application of CSLM in the area of materials science has been observed in the past decade [11]. In a CSLM image, contrast is built up due to the fact that local differences in refractive index act as scattering centers. For RDX [8] and HMX [9], it has been confirmed by scanning electron microscopic (SEM) observations of crystal surfaces that were obtained by cleaving the RDX and HMX crystals, that the presence of (micro)inclusions is responsible for the bright spots that have been observed in the CSLM images. CSLM images of the three selected RDX grades, showed evidence of small, (sub)micrometer-sized inclusions/voids with varying number densities, depending on the RDX product quality [8]. The inclusions in crystals originate from their production process, generally by means of crystallization, due to attrition and subsequent "healing" of the damaged locations, especially at the edges and corners of the larger crystals [12, 13].

[a] *A. E. D. M. van der Heijden, R. H. B. Bouma*
Department Energetic Materials
TNO, Organisation for Applied Scientific Research
P.O. Box 45
2280 AA Rijswijk, The Netherlands
**e-mail: antoine.vanderheijden@tno.nl*

[b] *A. E. D. M. van der Heijden*
Section Intensified Reaction and Separation Systems
Delft University of Technology
Leeghwaterstraat 39
2526 CB Delft, The Netherlands

The objective of this study is to investigate the influence of an explosion-driven deformation (without inducing a sustained deflagration or detonation) on the defect structure in RDX crystals embedded in a PBX (type AFX-575). Hereto, the interior of three different RDX crystalline grades were examined by means of CSLM after shock loading the PBXs containing these RDX grades using the explosion-driven deformation test. The obtained images were compared to the defect structure in the as-received RDX grades, embedded in an epoxy resin. An important advantage of CSLM is the fact that the defect structure within the crystals can be visualized at the microscale, whereas other experimental studies consider either the mesoscale [14,15], treating the PBX as a heterogeneous system consisting of crystalline particles embedded in a polymer binder, or the macroscale [16], where the PBX is described as a homogeneous material. By CSLM it is possible to analyze the changes in defect structure of the RDX crystals induced by the explosion-driven deformation.

2 Experimental

2.1 Selection of RDX Grades and PBX Formulation

Three RDX qualities from the Reduced Sensitivity RDX Round Robin program [5] were selected for further study, based on their shock initiation pressure and on a qualitative assessment (good, intermediate, bad) using optical micrographs of the RDX crystals immersed in a refractive index matched liquid. This Round Robin program showed that the RDX crystal quality significantly affected the shock sensitivity of PBXN-109 formulations each containing Class 1 RDX from the previously mentioned seven different sources [17].

The selected RDX samples are referred to as K1, K6, and K7. The characteristics of these three RDX grades are summarized in Table 1. Three PBX formulations, based on AFX-757, each containing one of the Class 1 RDX grades as well as ammonium perchlorate (AP) and aluminum in an HTPB polymer matrix, were cast-cured (see Table 2).

Table 1. Basic properties of the three Class 1 RDX grades used in the PBX formulations. Note that the data on the shock initiation pressure given in this table were obtained for PBXN-109 formulations, which differ in composition compared to the PBX compositions in this study.

PBX-ID	RDX grade and quality	Manufacturer	Shock initiation pressure [GPa]
RU187-1	K1; intermediate	BAe Royal Ordnance	5.06
RU186-1	K6; bad	Dyno Type II	3.86
RU185-1	K7; good	ADI	5.33

Table 2. Composition of the polymer-bonded explosive (PBX) formulations, derived from AFX-757.

Ingredient	Content [wt-%]
HTPB-based polymer binder[a)]	11.6
RDX, Class 1 (ca. 150 μm)[b)]	25.0
Aluminum <45 μm	33.0
Ammonium perchlorate (ca. 200 μm)	30.0
Processing aid	0.40
Total solid load	88.4

a) Polymer binder consists of: HTPB, plasticizer, isocyanate, curing catalyst and anti-oxidant. b) RDX batch K1, K6, or K7, see Table 1.

2.2 PBX Deformation

The deformation of the three PBX formulations has been described in detail by Bouma and van der Heijden [4]. Figure 1 shows the standard geometry. A 10 cm long steel cylinder filled with the PBX was sandwiched between two 5 cm long steel tubes filled with sand. The sand-filled cylinders provide an impedance match for the shock wave (see later) and thus a homogeneous deformation of the central PBX-filled cylinder. The cylinders were made out of St 52 and have an internal and external diameter of 60 and 70 mm, respectively. A layer of plastic explosive (Semtex 10) covering one-third of the circumference of the cylinder was used to drive the deformation of the steel-encased PBX. Both a 4 mm and 5 mm thick layer of Semtex 10 plastic explosive were used. A 4 mm thick rubber foam layer was put in between the Semtex 10 layer and the steel cylinder, and had to prevent a direct shock initiation of the

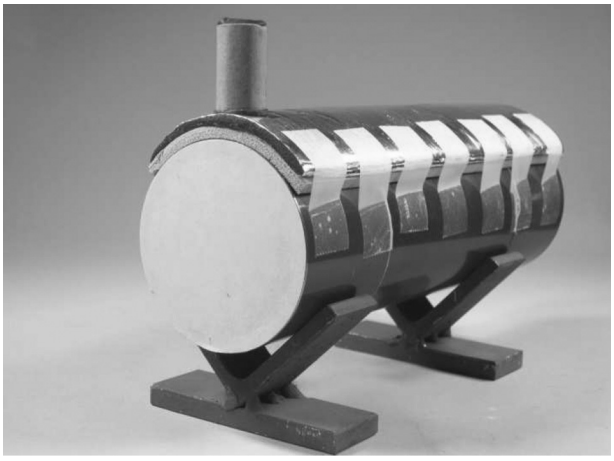

Figure 1. Explosion-driven deformation test with a plastic explosive layer (on top of the steel cylinders) deforming a steel-encased PBX. The steel case containing the PBX is shown in the middle and is sandwiched by two sand-filled steel casings. A 4 mm thick rubber foam layer was put in between the Semtex 10 layer and the steel cylinder, and had to prevent a direct shock initiation of the PBX. A detonator was inserted in a small amount of plastic explosive, visible at the top left, to initiate a detonation and start the deformation process.

PBX. A detonator was inserted in a small amount of plastic explosive to initiate a detonation and start the deformation process.

The maximum shock pressures are expected to be similar to the explosive deformation of PBXN-109, for which 0.66 and 0.84 GPa were obtained in numerical simulations with a 4 mm, and a 5 mm layer of Semtex 10 plastic explosive, respectively, and for an identical steel diameter and wall thickness [18]. From numerical simulations in a similar, 80 mm diameter geometry with RDX/HTPB compositions varying in RDX solid content from 65 to 80 wt-%, it was concluded that there was no significant influence of the material strength parameters of the central PBX fill upon deformation and that the sleeve might play an important role in the deformation process [19]. In another numerical study, again with similar geometry, a large variation of the Young's modulus of the PBX fill from 235 to 1000 MPa, led to an increase of the maximum pressure from ca. 0.01 to 0.3 GPa [20]. These data show that, although the mechanical properties of the PBX may be different, the pressures as a result of the shock loading remain well below the shock initiation pressure as the studied compositions are derived from AFX-757, which is an Extremely Insensitive Detonating Substance (EIDS). In order to pass the EIDS gap test [21] the shock initiation pressure must be at least 3.53 GPa. The detonation of the plastic sheet explosive will progressively deform the three steel cylinders. During the detonation of the layer of sheet explosive, the PBX is deformed as well and may react to a certain extent. After the deformation process, the PBX-filled steel cylinder was recovered and samples were taken from the deformed and unreacted part of the PBX formulation. The samples were cut from the center of the cone-shaped part of the deformed PBX that broke away from the original PBX cylinder. In total six samples were obtained: three PBX formulations containing RDX grade K1, K6, and K7 that were shock-loaded with either a 4 mm or a 5 mm thick plastic explosive layer.

2.3 Sample Preparation

Samples taken from the deformed, unreacted PBX formulations were embedded in an epoxy resin (EPO-THIN™ low viscosity epoxy, Buehler Ltd). The epoxy matrix was prepared by mixing EPO-THIN™ resin and EPO-THIN™ hardener in a 5 : 2 ratio by mass at a slightly elevated temperature (ca. 35 °C). The mixture was stirred for 2 min. After adding a small part of the deformed, unreacted PBX, the sample was transferred to a vacuum oven to allow gases to escape from the epoxy by alternately applying vacuum and atmospheric pressure. Afterwards, the sample was allowed to cure at ca. 35 °C during 3–4 h. After curing, the top layer of the epoxy resin was removed by polishing it with a coarse grade sandpaper (using water) until enough epoxy was removed to reach the embedded PBX sample. The sample was polished by gradually reducing the grit size of the sandpaper. The surface was finished using a Nylon disc and a 6 μm diamond oil-based suspension followed by a 3 μm diamond oil-based suspension and finally using a MasterTex® cloth. During the complete polishing procedure, the ammonium perchlorate (AP) crystals in the surface layer of the PBX sample were removed from the polymer matrix since the AP crystals dissolve in water. The RDX and aluminum particles retained in the PBX. The polishing procedure was monitored by means of optical microscopy, to check the surface of the cut and polished RDX crystals in between the subsequent polishing steps.

The original, as-received RDX crystals were also embedded in the EPO-THIN™ epoxy resin. After adding the RDX crystals to the mixture of epoxy resin and hardener, the suspension was stirred during 2 min to homogenize the suspension. The same procedure was applied as described above for preparing the PBX samples.

2.4 Characterization Method

A Leica TCS SL confocal system with a DM6000 B microscope was used to obtain confocal scanning laser microscopic (CSLM) images of the unreacted, shock-loaded PBX samples. A CSLM uses a point focus and a pinhole aperture (i.e. the confocal point) just before the reflected light from the sample reaches the detector, generally a photomultiplier tube. In this way out-of-focus light was rejected from the final image. The sample could be imaged by scanning the sample, focusing on a plane within the sample and moving to a deeper located, optical slice in the sample. In reflection mode the optical slices have a thickness of 0.50 μm. Local differences in refractive index within the RDX crystals were revealed as bright spots against a dark background. A series (stack) of 2D slices were imaged, starting approximately 15 μm below the surface of the RDX particle in order to avoid surface artefacts due to the cutting and polishing of the sample. In the majority of cases, an area of $375 \times 375\ \mu m^2$ (*xy* plane) and total stack thicknesses (*z* direction) varying from ca. 70 to 135 μm were visualized in this way.

For each of the six deformed and unreacted PBX samples, on the average ten to fifteen RDX crystals were first examined, and of these particles subsequently five representative crystals were selected for recording the CSLM images. Although a detailed statistical analysis was beyond the scope of this work, this approach assured that the features described in this paper were typical and representative for a reasonable number of examined crystals.

Although the CSLM technique records 2D slices, it can be considered a 3D imaging technique, since subsequently recorded 2D slices can be displayed sequentially, in this way moving through a 3D part of the crystal. This provides information on how the defects extend not only in the *xy* plane (lateral) but also in the *z* direction. This is clearly an advantage compared to other imaging techniques, like (conventional) optical microscopy or scanning electron microscopy.

As indicated, the original CSLM images show bright spots against a dark background. For improved contrast, the images were converted to grey/black spots against a white background.

3 Results and Discussion

Figure 2 shows an optical microscopy image of the PBX-K1 sample (deformed with a 4 mm thick explosive layer) after the last polishing step of the sample. The image shows RDX-K1 crystals (whitish, turbid particles) embedded in the HTPB-polymer matrix as well as holes (grey areas) that were left due to the washing of the AP particles from the PBX since AP dissolves in the water that was used to polish the PBX sample. The bright speckles in the image represent the aluminum particles. This image clearly shows the heterogeneous character of a PBX composition.

Prior to selecting and examining an RDX crystal by means of CSLM, the boundaries of the RDX particle were visualized by normal microscopy. In this way the position and location of the RDX crystal and its periphery (i.e. the particle-binder interface) in the subsequent CSLM image was established.

Inverted CSLM images are shown in Figure 3, Figure 4, Figure 5, Figure 6, Figure 7, and Figure 8 for the six deformed PBX formulations, one series containing either RDX from grade K1, K6, and K7 that was deformed with a 4 mm thick explosive layer (Figure 3, Figure 5 and Figure 7) and a similar series of PBXs that was deformed with a 5 mm thick explosive layer (Figure 4, Figure 6 and Figure 8). For all of the six PBX samples, the RDX crystals in the polymer binder are surrounded by regions causing severe light scattering. In the inverted images these regions show up as intensely black spots or areas, generally having a lateral dimension exceeding ca. 10 μm. The light scattering is caused by the presence of aluminum particles in the PBX formulation; these aluminum particles have a typical size smaller than 45 μm, which – due to this considerable differ-

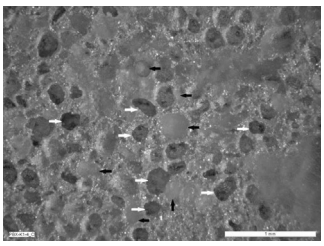

Figure 2. Optical microscopy image of PBX-K1 sample (deformed with a 4 mm thick explosive layer) after the last polishing step of the sample. The image shows RDX-K1 particles (indicated with black arrows) embedded in the HTPB-polymer matrix. The darker grey areas are holes (see white arrows) that were left due to the washing of the AP particles from the PBX since AP dissolves in the water that was used to polish the PBX sample. The bright speckles in the image represent the aluminum particles.

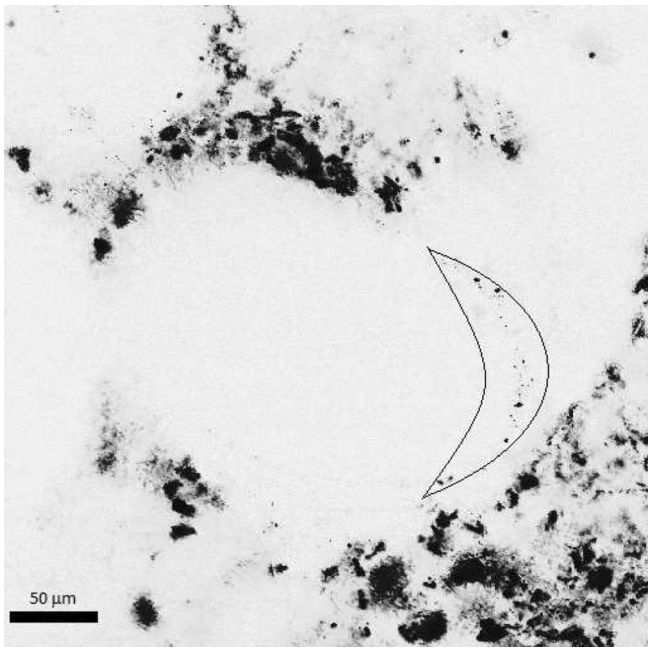

Figure 3. PBX-K1_4 mm, 375×375 μm^2. The larger, intensely black areas represent aluminum particles that surround the RDX particle, which is in the middle of this image. The curved right end of the RDX particle (i.e. the area enclosed by the black line) shows small inclusions in the periphery of the crystal.

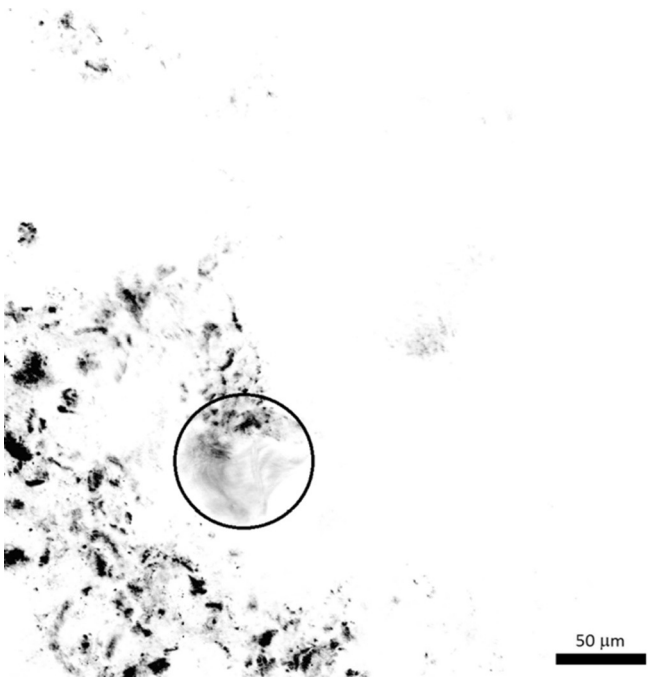

Figure 4. PBX-K1_5 mm, 375×375 μm^2. The area within the circle indicates an extended area of ca. 75×75 μm^2 (*xy* direction) that could be indicative of an area, where mechanical stress was induced by the shock loading of the PBX sample. The dimension of this particular area in the *z* direction is ca. 17 μm.

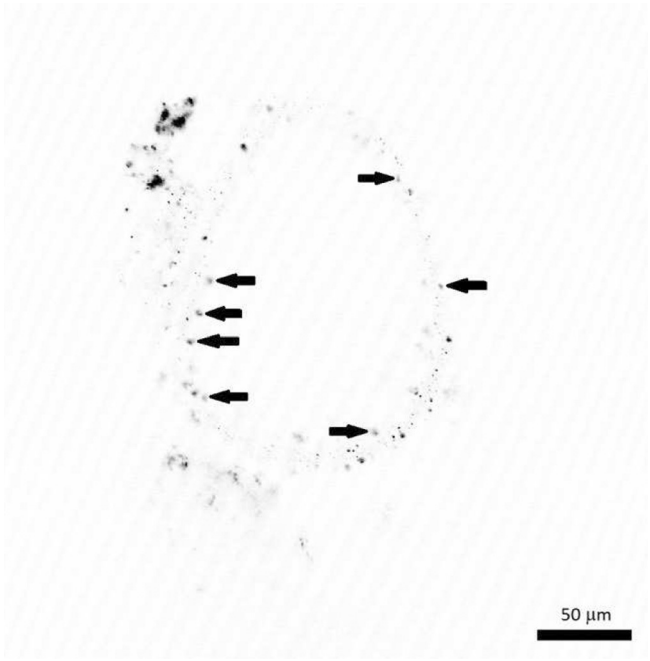

Figure 5. PBX-K6_4 mm, 375×375 μm^2. Apart from sharp-edged speckles, also blurred spots can be observed, some of which were indicated with the arrows. These blurred spots typically cover an area with a diameter of about 5 μm, which is ca. 5–10 times the typical diameter of a sharp-edged inclusion.

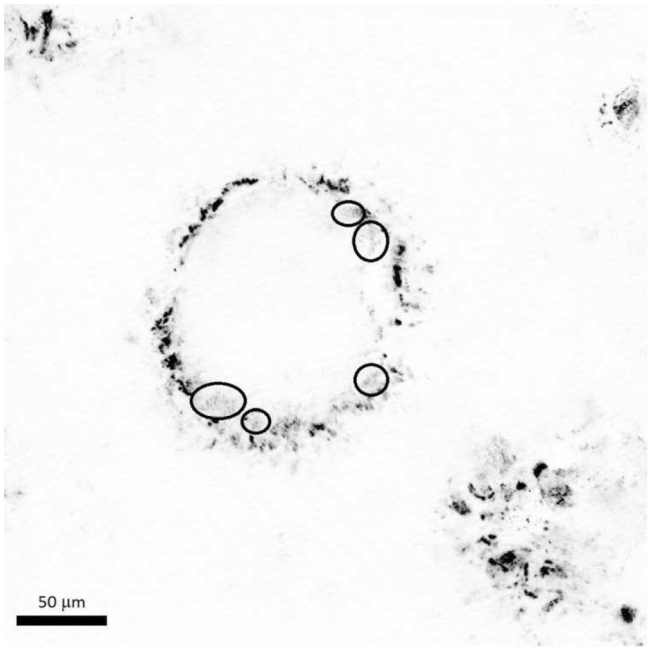

Figure 6. PBX-K6_5 mm, 375×375 μm^2. The RDX crystal in this example contains extended greyish areas (indicated by circles), mainly located in the periphery of the particle. These greyish areas could be indicative of mechanically induced stress.

ence in size – should be easily distinguishable from the much smaller defects present in the RDX crystals.

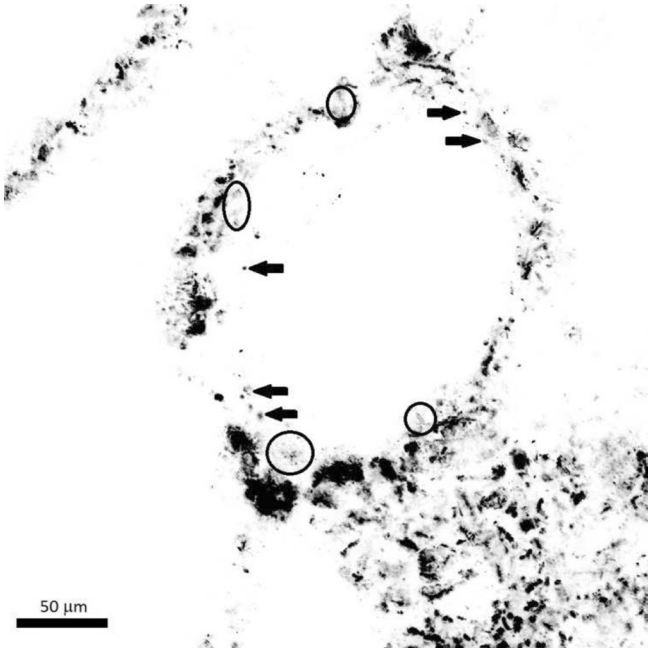

Figure 7. PBX-K7_4 mm, 375×375 μm^2. "Blurry" spots (arrows) as well as greyish areas (circles) can be observed.

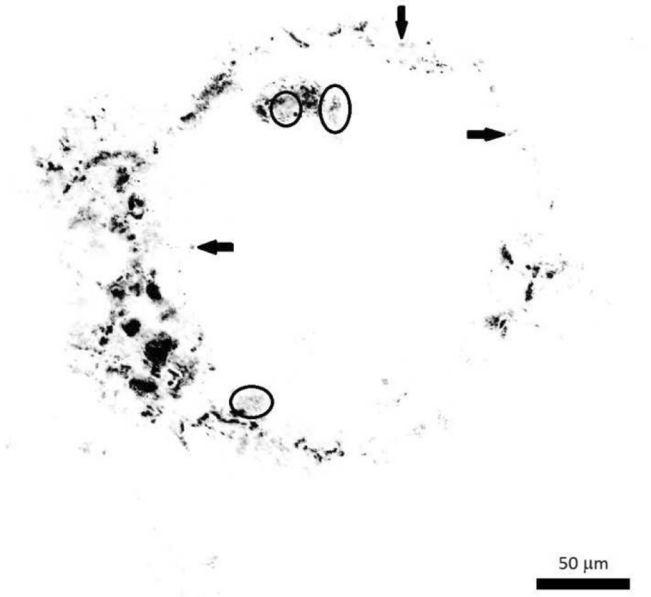

Figure 8. PBX-K7_5 mm, 375×375 μm^2. "Blurry" spots (arrows) as well as greyish areas (circles) can be observed.

By starting the CSLM scans at least 15 μm below the polished surface of the RDX crystals, artefacts from the applied polishing procedure were avoided. Furthermore, it is expected that the formulation processing, i.e. the mixing, casting, and curing of the PBX, did not affect the RDX crystals, since the formulation processing is a mild process with very limited mechanical forces applied to the solid particles present in the PBX mix. Although literature reported effects

of breakage of coarse AP particles in processing solid composite rocket propellants [22], these effects appear to be limited and the current experience is that at least for RDX, crystal breakage did not occur during the PBX formulation processing. Moreover, since specifically the defect structure within the RDX crystals is examined (rather than the macroscopic effects related to crystal breakage), this supports the assumption that the observed changes in the RDX defect structure solely arise from the explosion-driven deformation of the PBXs using the 4 mm and 5 mm thick Semtex explosive layer and not from other causes.

None of the RDX grades embedded in the deformed PBXs contained cracks. This is in line with the observations of the original RDX crystals embedded in the epoxy resin, so there appear to be no indications of the formation of cracks in the RDX crystals as a result of the applied shock loading.

The differences in refractive index are caused by inclusions or voids present in the crystals, as was confirmed previously for two different product qualities of HMX crystals [9] and for the original K1, K6, and K7 RDX grades [8] by comparing the CSLM images with scanning electron microscope (SEM) images of crystal surfaces obtained after cleaving the HMX and RDX crystals. The cleaved surfaces clearly showed the presence of small voids ranging in size from sub-μm to a few μm, pointing at the locations that are responsible for the different refractive index compared to the surrounding crystalline material.

Typical CSLM images of the original, as-received K1, K6, and K7 RDX grades have been extensively described [8]. RDX grades K6 and K7 generally show much more voids than grade K1. Inclusions in K1 generally have an individual character, but sometimes the inclusions appear to form a chain of separate inclusions; this is also observed in K7 crystals. Typical for K6 crystals is the presence of grayish areas, in addition to sharply edged speckles. The observed grayish areas in K6 crystals could be indicative of mechanically stressed areas. Specifically in K7, but also in K6, inclusions appear to be mainly localized in the periphery of the particles (as had been ascertained by normal microscopy prior to taking the CSLM image), whereas the central part is relatively "clean". The presence of inclusions mainly in the periphery of the crystals is in line with e.g. ammonium sulfate crystals [13]. This is due to the fact that during the production process (by means of solution crystallization) mainly the larger crystals suffer from collisions with other particles or with the stirrer in the crystallizer, leading to the attrition of small fragments from in particular the edges and corners of the crystals. These damaged areas are overgrown as a result of the existing supersaturation, forming inclusions [12,13]. When comparing subsequent CSLM slices 0.5 μm apart, generally new spots appear, while others disappear. This indicates that at least a number of the inclusions are in the order of 0.5 μm or smaller. This has been confirmed by SEM observations of cleaved crystal surfaces of RDX grades K1, K6, and K78 as well as those of two different product qualities of HMX [9].

When comparing the characteristic features in the CSLM images of the mechanically deformed PBX formulations with those of the original RDX batches, the following differences can be observed (see also Table 3): (1) in all of the RDX grades in the six deformed PBX formulations (i.e. three PBXs that were deformed using a 4 mm and three using a 5 mm thick layer of Semtex 10) though predominantly in K1, more extended, "cloudy" regions can be observed in addition to bright, sharply edged and blurred speckles. An example of such a "cloudy" region in K1 is indicated in the circle in Figure 4. The dimension of this particular area is ca. 75×75 μm^2 and extends ca. 17 μm in the direction perpendicular to the plane of the image. These "cloudy" regions appear to have been formed in practically inclusion-free areas of the original RDX crystal, since these type of "cloudy" regions are absent in the original, as-received K1 crystals [8]. (2) The speckles in the CSLM images of deformed PBXs containing the K6 and K7 crystals appear to be more "blurry" compared to those in the original K6 and K7 crystals. Examples of such blurred spots can be observed in Figure 5. Each of these blurred spots typically covers an area with a lateral dimension of about 5 μm, which is approximately 5–10 times the typical diameter of a sharp-edged inclusion. The typical extension of each blurred spot in the direction perpendicular to the plane of the image is comparable to the lateral dimensions, as was confirmed by comparing subsequent slices: the blurred spots are typically present in a stack of 20–30 CSLM slices (each slice is 0.5 μm apart from its adjacent slice).

Table 3. Overview of the different types of defects observed in the as-received RDX crystals and in the deformed, PBX-embedded RDX crystals.

Type of defect	Remark	Example
Sharp-edged, individual inclusions	Generally observed in as-received RDX crystals	[8]
Chain-like inclusions	Generally observed in as-received RDX crystals of K1 and K7	[8]
Greyish areas	Observed in as-received RDX K6 and in deformed PBX-embedded RDX crystals of K6 and K7	See e.g. Figure 6, Figure 7, and Figure 8 (indicated with circles)
"Blurry" spots	Observed in deformed PBX-embedded RDX crystals	See Figure 5, Figure 6, Figure 7, and Figure 8 (indicated with arrows)
"Cloudy" regions	Observed in deformed PBX-embedded RDX crystals, predominantly in K1	See e.g. Figure 4 (indicated with circle)

The blurred spots as well as the more extended "cloudy" regions observed in the different RDX grades, point at regions with a (slightly) different or gradually changing refractive index compared to the remaining part of the crystals, leading to the scattering of light in the CSLM imaging. Stress concentration at voids and void collapse are well-known for energetic materials under shock loading [23–26]. Therefore, it is expected that the local variations in refractive index are related to local variations in the density of the RDX through the Clausius-Mossotti equation [27] that – in turn – are the result of the mechanical stress induced by the shock loading. It is unclear whether the blurred spots originate from inclusions that were already present in the as-received crystals but obtained a blurry appearance due to the shock loading, or that these were newly generated as a result of the shock loading. The fact that the blurred spots are most abundant in the periphery of the crystal surface, similar to the inclusions in the original RDX crystals, might indicate that already existing inclusions become more intensely stressed due to the shock loading. If the blurred spots were newly generated by the shock loading, one would expect that these formed more or less homogeneously throughout the RDX particle and not primarily in the periphery of the particle.

The "cloudy" regions appear to have been formed in a practically inclusion-free part of the crystal. However, the fact that no inclusions are observed with CSLM, does not exclude the presence of other pre-existing defects, like dislocations. In the paper of Cawkwell et al. [28, 29] and also in the work of Rimoli et al. [30], mentioning is made of homogeneously nucleated hot spots, either as shear bands or slip lines providing likely initiation sites in defect-free crystals of RDX and PETN, respectively. In Ref. [29] large scale molecular dynamics simulations of the shock wave propagation in RDX showed that shock pressures in excess of 1.3 GPa favor homogeneous nucleation of partial dislocation loops within 10–50 nm of the shock front, which expand rapidly to fill the shock-compressed material with a high density of stacking faults. At pressures below 1.3 GPa, perfect dislocations will glide, multiply, and nucleate heterogeneously from pre-existing defects giving rise to a well-defined elastic-plastic response. Plate impact experiments using (111) oriented RDX crystals provided experimental support for this threshold of 1.3 GPa. Since the shock pressures in the current study are below the threshold of 1.3 GPa (i.e. 0.66 and 0.84 GPa), seems to suggest that the "cloudy" regions are caused by heterogeneously rather than homogeneously nucleated defects.

The observations provide for the first time experimental confirmation that mechanically stressed areas are formed around inclusions as a result of the explosion-driven deformation of PBXs. In addition most likely heterogeneously nucleated, shock-induced deformations were observed in RDX crystals by CSLM. At pressures exceeding the initiation shock pressure, these localized, mechanically induced deformation sites, may become hot spots, finally leading to initiation of the PBX.

4 Conclusions

The changes in the defect structure of RDX crystals, embedded in a PBX, after subjecting the PBX to an explosion-driven deformation, provide information on how a shock wave interacts with the RDX crystals and, more specifically, the defects present in the RDX crystals. The level of the shock loads investigated in this study, appears to be too low to induce cracks in the RDX crystals, but it is sufficiently high to primarily interact with the inclusions/voids already present in the original, as-received crystals, giving rise to a significantly increased number of spots attaining a blurry appearance, contrary to the small, usually sharply edged spots in the original crystals. The fact that these spots in the CSLM images are predominantly localized in the periphery of the crystals, similar to the inclusions that are present in the original crystals, is an indication that the formation of new defects (inclusions/voids) in the crystals is limited or even absent, assuming that this would take place more or less homogeneously throughout the crystal volume. An exception to this is the appearance of cloudy regions, mainly in practically inclusion-free areas of RDX K1 grade crystals that could point at areas in the crystal with a (gradual) change in refractive index due to local changes in the density of the material mechanically induced by the shock loading. For the first time experimental confirmation has been obtained supporting the results from several molecular dynamics simulation studies on the propagation of shock waves through RDX crystals containing a void, indicating that the inclusions and voids present in the original RDX crystals act as preferred locations, around which mechanical deformations are induced as a result of the interaction with the passing shock wave. Similarly, experimental evidence has been obtained of most likely heterogeneously (from pre-existing defects) nucleated shock-induced deformations in previously inclusion-free, though probably not dislocation-free areas in RDX crystals. At pressures exceeding the initiation shock pressure, these localized, mechanically induced deformation sites may become hot spots, finally leading to initiation of the PBX.

Acknowledgments

The authors acknowledge support from the U.S. Defense Threat Reduction Agency under project award HDTRA1-10-1-0078. Mrs A. M. A. van der Laan is acknowledged for assistance during the measurements with the confocal scanning laser microscope at the Department of Molecular Cell Biology, Leiden University Medical Center (LUMC), The Netherlands.

References

[1] I. G. Wallace, Spigot Intrusion, *26th Department of Defense Explosives Safety Seminar*, Miami, FL, USA, 16–18 August, **1994**.

[2] S. K. Chidester, C. M. Tarver, R. Garza, Low Amplitude Impact Testing and Analysis of Pristine and Aged Solid High Explosives, *11th International Detonation Symposium*, Snowmass, CO, USA, 31 August–4 September, **1998**.

[3] H. W. Sandusky, G. P. Chamber, V. J. Carlson, Setback Simulation of Fielded and Candidate Explosive Fill for 5″/54 Guns, *JANNAF Propulsion Systems Hazards Subcommittee Meeting*, CPIA Publ. 681, 7–11 December, **1998**, p. 137–145.

[4] R. H. B. Bouma, A. E. D. M. van der Heijden, The Effect of RDX Crystal Defect Structure on Mechanical Response of Polymer-Bonded Explosive, *Propellants Explos. Pyrotech.* **2016**, published online, DOI: 10.1002/prep.201500222.

[5] R. M. Doherty, D. S. Watt, Relationship Between RDX Properties and Sensitivity, *Propellants Explos. Pyrotech.* **2008**, *33*, 4.

[6] A. E. D. M. van der Heijden, C. P. M. Roelands, Y. L. M. Creyghton, E. Marino, R. H. B. Bouma, J. H. G. Scholtes, W. Duvalois, Energetic Materials: Crystallization, Characterization and Insensitive Plastic-Bonded Explosives, *Propellants Explos. Pyrotech.* **2008**, *33*, 25–32.

[7] R. H. B. Bouma, A. G. Boluijt, H. R. Verbeek, A. E. D. M. van der Heijden, On the Impact Testing of Cyclotrimethylene Trinitramine Crystals with Different Internal Qualities, *J. Appl. Phys.* **2008**, *103*, 093517.

[8] R. H. B. Bouma, W. Duvalois, A. E. D. M. van der Heijden, Microscopic Characterization of Defect Structure in RDX Crystals, *J. Microsc.* **2013**, *252*, 263 – 274.

[9] A. E. D. M. van der Heijden, R. H. B. Bouma, Crystallization and Characterization of RDX, HMX and CL20, *Cryst. Growth Des.* **2004**, *4*, 999–1007.

[10] S. W. Paddock, Principles and Practices of Laser Scanning Confocal Microscopy, *Mol. Biotechnol.* **2000**, *16*, 127.

[11] D. B. Hovis, A. H. Heuer, The Use of Laser Scanning Confocal Microscopy (LSCM) in Materials Science, *J. Microsc.* **2010**, *240*, 173.

[12] A. E. D. M. van der Heijden, J. P. van der Eerden, G. M. van Rosmalen, The Secondary Nucleation Rate: A Physical Model, *Chem. Eng. Sci.* **1994**, *49*, 3103–3113.

[13] R. OMeadhra, *Modelling of the Kinetics of Suspension Crystallizers, a New Model for Secondary Nucleation*, PhD Thesis, Delft University of Technology, Delft University Press, Delft, **1995**.

[14] J. Vial, D. Picart, P. Bailly, F. Delvare, Numerical and Experimental Study of the Plasticity of HMX During a Reverse Edge-On Impact Test, *Model. Simul. Mater. Sci. Eng.* **2013**, *21*, 045006.

[15] S. M. Walley, *Strain Localization in Energetic and Inert Granular Materials, in: Adiabatic Shear Localization – Frontiers and Advances* (Eds.: B. Dodd, Y. Bai), 2nd ed., Elsevier, Amsterdam, **2012**.

[16] J. Furmanski, P. Rae, B. Clements, Moderate Velocity Ball Impact of a Mock High-Explosive, in: Dynamic Behavior of Materials, Volume 1, *Conference Proceedings of the Society for Experimental Mechanics Series*, **2013**, pp. 409–415.

[17] D. S. Watt, R. M. Doherty, L. Nock, *RS-RDX Round Robin (R4) Preliminary Results Analysis*, NATO-MSIAC Report L-127, Brussels, Belgium, **2006**.

[18] B. Meuken, M. Martinez Pacheco, H. J. Verbeek, R. H. B. Bouma, L. Katgerman, Shear Initiated Reactions in Energetic and Reactive Materials, *Mater. Res. Soc., Symp. Proc.*, Vol. 896, 0896-H06-06, **2005**.

[19] P. J. König, F. J. Mostert, The Results of a Deformable Warhead Technology Exercise, *20th International Symposium on Ballistics*, Orlando, FL, USA, 23–27 September, **2002**.

[20] S. Dell'Amore Fachinetti, Numerical Models for Aimable Warhead, in: *EnginSoft Newsletter Year 10*, no. 3, **2013**, pp. 11–16.

[21] *Recommendations on the Transport of Dangerous Goods, Manual of Tests and Criteria*, ST/SG/AC.10/11/Rev.4.

[22] A. C. Hordijk, A. E. D. M. van der Heijden, *Mixing, in: Energetic Materials – Particle Processing and Characterization* (Ed.: U. Teipel), Wiley-VCH, Weinheim, **2005**.

[23] L. Tran, H. Udaykumar, Simulation of Void Collapse in an Energetic Material, Part 1: Inert Case, *J. Propul. Power* **2006**, *22*, 947–958.

[24] L. Tran, H. Udaykumar, Simulation of Void Collapse in an Energetic Material, Part 2: Reactive Case, *J. Propul. Power* **2006**, *22*, 959–974.

[25] M. L. Baer, in: *Shock Wave Science and Technology Reference Library* (Ed.: Y. Horie), Vol. 2, chapter 8, Springer, Heidelberg, **2006**.

[26] A. Kapahi, H. S. Udaykumar, Dynamics of Void Collapse in Shocked Energetic Materials: Physics of Void–Void Interactions, *Shock Waves* **2013**, *23*, 537–558.

[27] R. P Feynman, R. B. Leighton, M. Sands, in: *The Feynman Lectures on Physics*, Vol II, 6th printing, Chapter 32, Addison-Wesley Longman, Amsterdam, **1977**.

[28] M. J. Cawkwell, T. D. Sewell, L. Zheng, D. L. Thompson, Shock-Induced Shear Bands in an Energetic Molecular Crystal: Application of Shock-Front Absorbing Boundary Conditions to Molecular Dynamics Simulations, *Phys. Rev. B* **2008**, *78*, 014107.

[29] M. J. Cawkwell, K. J. Ramos, D. E. Hooks, T. D. Sewell, Homogeneous Dislocation Nucleation in Cyclotrimethylene Trinitramine under Shock Loading, *J. Appl. Phys.* **2010**, *107*, 063512.

[30] J. J. Rimoli, E. Gürses, M. Ortiz, Shock-Induced Subgrain Microstructures as Possible Homogeneous Sources of Hot Spots and Initiation Sites in Energetic Polycrystals, *Phys. Rev. B* **2010**, *81*, 014112.

Received: October 7, 2015
Revised: February 4, 2016
Published online: April 28, 2016

